PAPER AAS 96-140

THE ORBITAL MOTION OF THE MARTIAN SATELLITES: AN APPLICATION OF ARTIFICIAL SATELLITE THEORY

Robert A. Jacobson

Jet Propulsion Laboratory
California Institute of Technology
Pasadena, California

AAS/AIAA Space Flight Mechanics Meeting

Austin, Texas 12-15 February 1996

AAS Publications Office, P.O. Box 28130, San Diego, CA 92198

THE ORBITAL MOTION OF THE MARTIAN SATELLITES: AN APPLICATION OF ARTIFICIAL SATELLITE THEORY

Robert A. Jacobson[1]

This paper describes an extended Sinclair-Morley analytical theory for the Martian satellites. The theory's foundation is the artificial satellite theory of Brouwer. In the paper we outline the original theory, present our modifications and additional terms, and compare the theory with numerical integration. We also provide a comparison with one of the other competing dynamical Martian satellite theories, namely the ESAPHO/ESADE theory of Chapront-Touzé.

Introduction

The Martian satellites, Phobos and Deimos, were discovered in 1877 by Asaph Hall. They move in close, nearly circular orbits which are slightly inclined to the Martian equator. Their principal orbital perturbations are due to the non-spherical nature of the Martian gravity field, but they are also significantly affected by solar perturbations. Planetary perturbations, however, are negligible, and because of their small masses their mutual perturbations are negligible as well. The studies of their motions from observations have found evidence of a secular acceleration in Phobos' orbit, and a similar acceleration in Deimos' orbit is suggested but much less certain. Sharpless[13] determined such a large value for Phobos' acceleration that it implied an impact with Mars within a few tens of millions of years. One explanation for the source of that large acceleration (atmospheric drag on hollow bodies) led to the speculation that the Martian satellites were in fact artificial bodies (see Ref. 14). Perhaps it is therefore appropriate to consider employing artificial satellite theory to describe their orbits.

Since the satellites' discovery a number of analytical theories have been developed to represent their orbital motions. These early theories were kinematical in nature designed primarily to provide positions for astronomical observation. In 1972 a dynamical theory created by Sinclair[15] appeared. This work was inspired by the artificial satellite theory of Brouwer[2] although Sinclair's variation of parameters approach more closely matched Kozai's approach[9,10] rather than that of Brouwer who favored the von Zeipel technique. Artificial satellite theory has the Earth's (planet's) equator as its reference plane. However, when the Martian equator is used for the Martian satellites, large periodic perturbations due to the Sun appear in the inclinations and nodes, especially for Deimos. Sinclair found that by modifying the theory and referring the elements to the Laplacian planes[7,11], those perturbations could be avoided. The satellite orbits process almost uniformly on the Laplacian planes because the latter are defined such that the periodic perturbations due to the Martian oblateness and Sun just cancel each other. Included in the theory is a secular acceleration term in the satellites'

[1]Jet Propulsion Laboratory/California Institute of Technology

longitudes to account for the possibility of a change in their mean motions. The small observed acceleration for Phobos is currently attributed to the gravitational attraction of the tidal bulge raised by it on Mars. No statistically significant acceleration has yet been observed for Deimos.

Sinclair's original theory was sufficiently accurate to process Earthbased observations, but when observations with an accuracy of nearly 2 km became available from spacecraft, an improvement was needed. Sinclair[16] expanded his theory to include a few more terms, especially an overlooked long period term in the longitude of Deimos pointed out by Born and Duxbury[1] and second order terms in the longitude of Phobos found by Chapront-Touzé[4]. At this point the theory was presumed accurate to better than 1 km. Morley[12] then extended Sinclair's work by increasing the accuracy of the existing terms describing the secular and periodic perturbations and by adding a number of previously omitted smaller terms. He also included terms to account for perturbations due to the tesseral harmonics of the Mars gravity field and short period solar perturbations as well as additional second order effects in the longitude. Based on a comparison with a 60 day numerical integration, Morley estimated his version of the theory to be accurate to better than 100 m.

We have adopted the Sinclair-Morley theory as the basis for Martian satellite ephemerides being developed in support of JPL's Mars Exploration Program. The theory's accuracy is more than sufficient for currently projected spacecraft operations needs. Moreover, its fully analytical nature permits modifications and updates in light of future observations and improvements in the Martian gravity field parameters. As part of the initial verification of theory, we compared our implementation to a 60 day numerical integration and found, as did Morley, an accuracy better than 100 meters. We then extended the comparison to 20 years for Phobos and 150 years for Deimos. The former comparison covered a time span about 1.8 times the longest period in the Phobos theory, and the latter covered about 1.5 times the longest period in Deimos theory. These long period comparisons suggested that the theories were good to only 300 meters for Phobos and 900 meters for Deimos. Although these accuracies are more than adequate for our current purpose, we made an attempt to recover the 100 meter accuracy by modifying the theory.

This paper describes our extended Sinclair-Morley theory for the Martian satellites. It outlines the original theory, presents the modifications and additional terms, and compares the theory with numerical integration. We also provide comparison with one of the other competing dynamical Martian satellite theories, namely the ESAPHO/ESADE theory[4,5,6].

Sinclair-Morley Theory

The orbits of the satellites are specified in terms of their osculating elements. Originally Sinclair and Morley used a set of equinoctial elements defined by:

$$
\begin{aligned}
G_1 &= a \\
G_2 &= e \cos \varpi \\
G_3 &= e \sin \varpi \\
G_4 &= 2 \sin \frac{I}{2} \sin \Omega \\
G_5 &= -2 \sin \frac{I}{2} \cos \Omega \\
G_6 &= \lambda
\end{aligned}
$$

where $a, e, \varpi, \lambda, I, \Omega$ are the classical elements semi-major axis, eccentricity, longitude of periapsis, mean longitude, inclination, and longitude of ascending node, respectively. Our implementation of the theory is in terms of the more familiar (Broucke) equinoctial elements:

$$E_1 = a$$
$$E_2 = e \sin \varpi$$
$$E_3 = e \cos \varpi$$
$$E_4 = \lambda$$
$$E_5 = \tan \frac{I}{2} \sin \Omega$$
$$E_6 = \tan \frac{I}{2} \cos \Omega$$

The relationship between the two sets of equinoctial elements is straightforward. Equinoctial elements are preferred over the classical Keplerian elements because the small eccentricities and inclinations of the orbits cause the location of the node and pericenter to be poorly defined and difficult to determine from observations.

The orbit of each satellite is referred to its Laplacian plane, the plane on which the orbit plane precesses almost uniformly. The choice of this plane introduces a large periodic variation into satellite's inclination and nodal longitude due to Mars' oblateness which just cancels an analogous variation due to the Sun. The Laplacian planes share a common node with the Mars equator and Mars orbital plane and precess along with the equator under the action of the Sun. Hence, the theory is actually developed in a rotating coordinate system. The geometry of the various planes is shown in Figure 1. The additional angles appearing in that figure are: i', Ω', the inclination and node of the Mars orbit with respect to the ecliptic; i, the inclination of the Mars equator to the Laplacian plane; I', the inclination of the Mars orbit to the Laplacian plane; Q, the obliquity of the Mars equator; $1'$ the ascending node of the Mars equator on the Mars orbital plane; ϕ the location of the Mars prime meridian measured from the ascending node of the Mars equator on the Mars orbit. The latter two angles are assumed to vary linearly with time ($P' = P'_0 + \dot{P}'t$ and $\phi = \phi_0 + \dot{\phi}t$) due to the precession of the equator and rotation of the planet. The inclinations to the Laplacian plane are related by $Q = I' + i$.

The theory is essentially an analytical variation of parameters solution for the equations of motion in terms of the classical elements (Ref. 3) with perturbations due to the asphericity of the Martian gravity field, the Sun's gravity and the precession of the Mars equator. Perturbations from the other planets and from interactions between the satellites are negligible. The expressions for the classical element variations are combined to obtain those for the equinoctial elements. Sinclair[15] and Morley[12] provide the details of the development.

The base orbits or zero order solution of the equations include only the effects of the secular perturbations. Consequently, three elements are constant and three vary with time, t:

$$a = a_0$$
$$e = e_0$$
$$\bar{\varpi} = \varpi_0 + n'\beta t$$
$$\bar{\lambda} = \lambda_0 + n_0(1 + \alpha)t + m t^2$$
$$I = I_0$$
$$\bar{\Omega} = \Omega_0 + n'\gamma t$$

where an element with zero subscript is its epoch value (i.e., at $t = 0$). The mean longitude expression includes a quadratic term to account for the observed secular acceleration of Phobos currently attributed to tidal forces. The parameter n' is the mean motion of Mars and the parameter n_0 is the satellite's Keplerian mean motion which is related to the semi-major axis through the gravitational parameter of Mars μ

$$n_0^2 a_0^3 = \mu$$

Hence, there are only 6 independent epoch elements. The Appendix provides the complete expressions for secular perturbations, α, β, and γ.

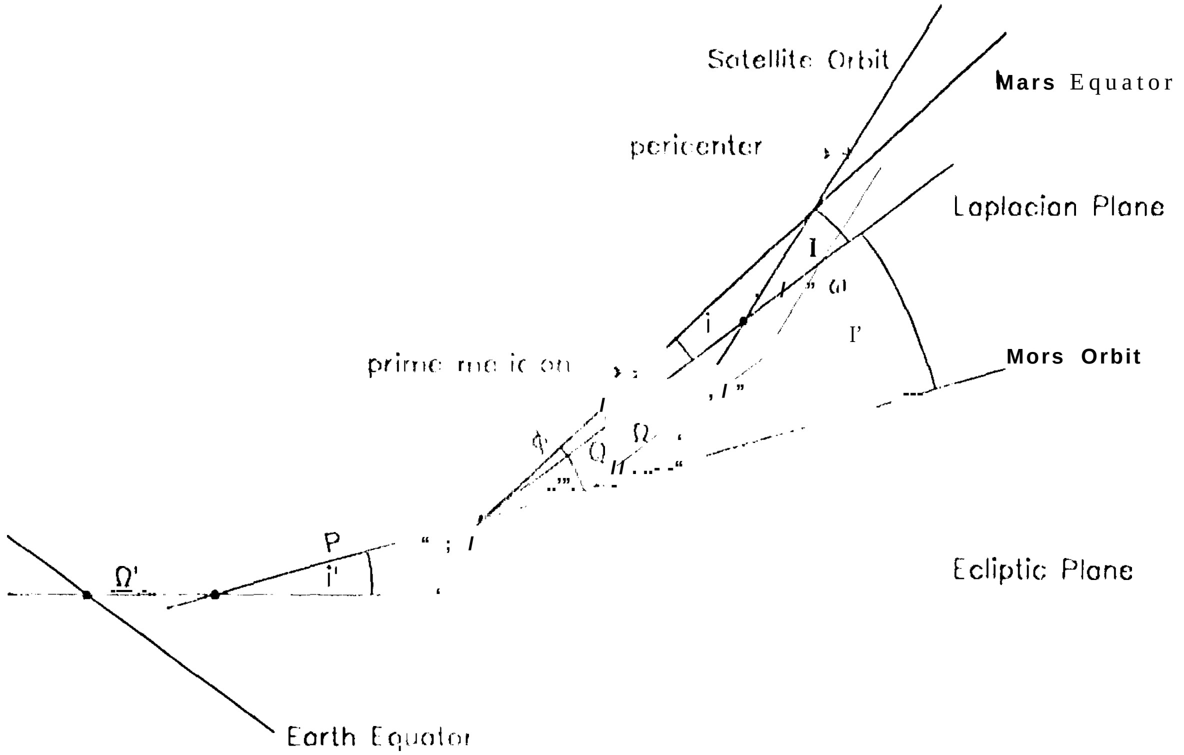

Figure 1: Satellite Orbital Plane Geometry

The inclination of the Laplacian plane to the Martian equator is computed by setting the largest first order periodic perturbation in the satellite inclination to zero. This process leads to the relation

$$\mathcal{A}\sin 2i = \mathcal{B}\sin 2(Q - i)$$

Sinclair[15] gives expressions for $\mathcal{A}$ and $\mathcal{B}$. Our extension of those expressions is

$$\mathcal{A} = \left(\frac{\mu}{a_0^3}\right)\left[2\frac{J_2R^2}{p_0^2} - 5\frac{J_4R^4}{p_0^4}\left(1 + \frac{3}{2}e_0^2\right)\right]\sqrt{1 - e_0^2}$$

$$\mathcal{B} = \left(\frac{\mu'}{a'^3}\right)\left(1 - e'^2\right)^{-3/2}\left(1 + \frac{3}{2}e_0^2\right)$$

where

p_0	=	$a_0\,(1 - e_0^2)$
J_2, J_4	=	second and fourth zonal harmonics of the Martian gravity field
R	=	equatorial radius of Mars
μ'	=	gravitational parameter of the Sun
a'	=	semi-major axis of the Mars orbit
e'	=	eccentricity of the Mars orbit

We determine the epoch values of the equinoctial elements by fitting the computed orbits to observations. In practice, however, it is much better to estimate the orbit's 'observed' mean motion $\bar{n}$ rather than its semi-major axis a_0 and then compute the latter together with the Keplerian mean motion n_0 from the implicit relation

$$
\begin{aligned}
\tilde{n} &= n_0(1+\alpha) \\
\mu &= n_0^2 a_0^3
\end{aligned}
$$

The parameter α is a function of a_0, e_0, I_0, n_0, and i. Since the inclination i is also a function of a_0, e_0, and n_0, it is found from

$$
\tan 2i = \frac{\mathcal{B}\sin 2Q}{\mathcal{A}+\mathcal{B}\cos 2Q}
$$

as an intermediate step in the a_0 computation. A straightforward Newton iteration scheme suffices to obtain a_0 given $\tilde{n}$, e_0, and I_0.

The first order solution or perturbed orbit follows from the standard variation of parameters by substituting the zero order solution into the equations of motion and integrating. Morley[12] found that some second order solution terms for the mean longitude were also needed for an accurate description of the orbit. With one exception the second order effects arise from an interaction of the zero order secular perturbation with first order long period perturbations in eccentricity and inclination. The exception applies to Deimos where a large first order long period perturbation in mean longitude interacts with the short period $J_{2,2}$ perturbation. We have found it necessary to include an additional long period second order term in the both the inclination and node. The development of this term is discussed later in this paper.

Although the perturbed solution is developed in terms of classical elements, for computational purposes, as indicated earlier, we transform it into equinoctial elements. The final theory describing the osculating elements has the form

$$
\begin{aligned}
E_1 &= E_{10} + \sum \Delta_1 E_1 \\
E_2 &= E_{20}\cos n'\beta t + E_{30}\sin n'\beta t + \sum \Delta_1 E_2 \\
E_3 &= E_{30}\cos n'\beta t - E_{20}\sin n'\beta t + \sum \Delta_1 E_3 \\
E_4 &= E_{40} + \tilde{n}t + mt^2 + \sum \Delta_1 E_4 + \Delta_2 E_4 \\
E_5 &= E_{50}\cos n'\gamma t + E_{60}\sin n'\gamma t + \sum \Delta_1 E_5 + \Delta_2 E_5 \\
E_6 &= E_{60}\cos n'\gamma t - E_{50}\sin n'\gamma t + \sum \Delta_1 E_6 + \Delta_2 E_6
\end{aligned}
$$

where the $\Delta_1 E_i, i = 1\ldots6$ are the first order perturbations and $\Delta_2 E_i, i = 4\ldots6$ are the second order perturbations. The Appendix contains complete expressions for the secular perturbations and expressions for all of the terms we introduced to extend the theory. Morley[12] provides the remainder of the terms (which are easily converted to our form of the equinoctial elements).

Comparison with Numerical Integration

Sinclair designed his original theory to account for all perturbations with effects larger than 1 part in 10^4 or about 1 km for Phobos and 2 km for Deimos. His later work sought to have sub-km accuracy, and when he compared it with a [illegible] day numerical integration, he found agreement to about 320 meters for Phobos and 820 meters for Deimos. Morley's extension attempted to bring in all terms with magnitudes greater than [illegible] meters for either satellite. His comparison with a 60 day numerical integration showed an accuracy of about [illegible] meters, however, he acknowledged that this comparison interval was too short to reveal the effects of the long period terms.

For Phobos the longest period perturbations, which are due to the Sun, have a period of the order of 4070 days (11 years), and for Deimos the dominant perturbation is a combined J_2 and solar effect with a period of about 19,920 days (5.5 years). In order to examine the theory accuracy with respect to these long period terms we made a comparison with integrations of 7300 days (20 years) for Phobos and 29,220 days (80 years) for Deimos. Initially we fit the integrated orbits to the theories, thus providing integrated orbits having osculating elements representative of the actual satellite orbits. The integrations were perturbed by a full 8 by 4 Martian gravity field (8 zonal and 4 tesseral harmonics), by Jupiter, and by the Sun. Next, with the integrated orbits held fixed, we adjusted the epoch elements of the theories to improve the match between integration and theory. Figures 2-7 show the differences in the local downtrack, radial, and out of the orbit plane directions. For both satellites the maximum error in the downtrack direction is of the order of 300 meters, radial errors are in the 100 to 200 meter range as is the Phobos out of plane error, but the Deimos out of plane error is nearly 1 km.

As it stands the long period accuracy is approximately that of Sinclair's final design. To reach Morley's desired accuracy goal the Phobos theory requires nearly a factor of 3 improvement and that of Deimos requires nearly an order of magnitude improvement.

Extended Theory

In our examination of the theory, we concluded that much of the accuracy could be recovered with improvements in the secular perturbations. To that end we introduced more complete expressions for the existing terms, replaced the J_2^2 term with that of Kinoshita[8], and added the third order J_3^2/J_2, J_2^3, and J_2J_4 terms from Kinoshita[8]. Tables 1 and 2 show the contributions of the various terms to the overall secular perturbations. Note that for Phobos, the J_3^2/J_2 term exceeds that of the precession, and the J_2J_4 term is comparable to it. Also, with the exception of Phobos J_2^3 term, the added third order terms are larger than the J_8 which is the smallest term considered by Morley.

Table 1
PHOBOS SECULAR PERTURBATION - deg/day

Source	Mean longitude	Pericenter	Node
J_2	0.8679784316	0.43395[illegible]	0.4342053958
J_4	0.0011202227	0.0011[illegible]	-0.0011215082
J_2^2	0.0008351762	0.000581[illegible]	-0.0004177346
Sun	-0.0001796583	[illegible]	-0.0001348003
J_6	-0.0000534092	-0.0000801138	0.0000801138
J_3^2/J_2	-0.0000000050	[illegible]	[illegible]
Precession	0.0000052168	0.0000052168	0.0000052168
J_2J_4	0.0000030198	0.00000[illegible]	-0.0000023727
J_8	0.0000007262	0.0000014523	-0.0000014523
J_2^3	0.0000009000	0.0000007393	0.0000004821
Total	0.8697106207	[illegible]	-0.4358057763

Since they were readily available we also added the J_5 periodic perturbations from Brouwer[2] which introduce about a 30 meter effect for Phobos. To further improve the Deimos downtrack, we replaced the original long period mean longitude perturbation due to J_2 and the Sun with a more complete expression. Finally to improve the Deimos out of plane, we included some neglected long period solar perturbation terms which have effects of up to 200 meters, introduced a more complete expression for the Laplacian plane inclination, and added a 100 meter second order term to both the inclination and node. The new expressions and additional terms are given in the Appendix. The Laplacian plane inclination expression appeared in an earlier section.

The additional second order terms arise from interactions of first order short period perturbations with the first order short period perturbations in eccentricity and periapsis longitude due to J_2. The short period terms satisfies equations of the form

$$\frac{dI}{dt} \sim n_0 \cos I \sin \Omega \, e \cos(\lambda - \varpi)$$

$$\frac{d\Omega}{dt} \sim n_0 \frac{\cos 2I}{\sin I} \cos \Omega \, e \cos(\lambda - \varpi)$$

Because of the small eccentricity of Deimos, the above have a negligible first order short period contribution. However, as a result of the J_2 perturbation we have

$$e \cos(\lambda - \varpi) \sim \frac{3}{2} \frac{J_2 R^2}{a_0^2}$$

which when introduced into the above yields

$$\frac{dI}{dt} \sim \frac{3}{2} n_0 \frac{J_2 R^2}{a_0^2} \cos I \sin \Omega$$

$$\frac{d\Omega}{dt} \sim \frac{3}{2} n_0 \frac{J_2 R^2}{a_0^2} \frac{\cos 2I}{\sin I} \cos \Omega$$

leading to a long period second order term.

Table 2
DEIMOS SECULAR PERTURBATIONS - deg/day

Source	Mean longitude	Pericenter	Node
J_2	0.0350037327	0.01749774?6	-0.0175226848
Sun	-0.00072'(2s(1s	0.00[illegible]5 [illegible]5 [illegible]68	-0.0005457846
J_4	0.00000'7191s	0.0000007 [illegible]18	-0.(111000'(2142
Precession	0.0000052 [)4 I	0.00000052[illegible]	().(111 00052541
J_2^2	0.0000053793	0.0000037[illegible]5	0.0000026922
J_6	-0.0000000[)5(0	0.00[illegible]0[illegible]0[illegible]825	0.0000000826
J_3^2/J_2	-0.00000000(12	[1 0000001?0	0.0000000473
J_2J_4	0.0000000031	(1 0000[illegible]0[illegible]1[illegible]3	(). () 000000024
J_2^3	0.0000000009	[1 00000008	0.0000000005
J_8	0.00000000(1 1	(1 (1(000002	-0.0000000002
Total	0.0342942?(0	(1 0180?58946	0.0180730896

To **test** the extended theory, we fit it to the same integration as the original. Figures **8-13** show the differences in the local downtrack, radial, and out of the orbit plane directions. For Phobos there **is** considerable improvement with the maximum error in the downtrack direction of the order of 150 meters and the radial and out of plane errors less than 100 meters. On the other hand, for Deimos the out of plane error is reduced to about 500 meters but the downtrack and radial errors remain essentially unchanged.

Because of the importance of the secular perturbations in the long term motion of the satellites, we augmented the extended theory with empirical corrections to the pericenter and node rates. These corrections are designed to account for inaccuracies in the analytical expressions for the rates, and their values will be ultimately be estimated from observations. As part **of** our testing **of** the theory, we decided **to** include these corrections in another fit to the integration. In addition, we included an adjustment to the angle Q, the obliquity of the Mars equator, to allow for a possible mismatch between the theory and integration. Table 3 provides the values of the rate and equator corrections. Figures **14-19** display the results of the exercise. Note that the Phobos downtrack error has dropped below the 100 meter level suggesting that further refinement of the analytical expression for pericenter rate may be all that is required to achieve that level without the empirical correction. The Deimos out of plane error has dropped to about 200 meters as a consequence of the node rate and Q corrections. However, the Q correction is detrimental to the Phobos out of plane error, increasing it to slightly more than 100 meters.

The Deimos downtrack error improved only slightly.

We believe that the Q correction is not valid, i.e., the location of the Mars equator in the theory is correct, and that the main problem remaining with the theory is an inadequate description of the Deimos out of plane motion. And, since to date has found neither errors in the implementation nor omitted but significant first order terms. Any improvement would appear then to require the development of additional second order terms. We also conjecture that much of the remaining Deimos downtrack error is a byproduct of the out of plane error. The downtrack motion is dominated by the long period mean longitude J_2 solar perturbation which is a strong function of the inclination, node, and node rate. Any inaccuracies in the values of those parameters as a result of the incomplete out of plane motion description would directly affect the downtrack error.

Table 3
SECULAR PERTURBATION AND EQUATOR CORRECTIONS

Parameter	Value	Units
Phobos pericenter rate	0.0000024987	deg/day
Phobos node rate	0.0000026705	deg/day
Deimos pericenter rate	-0.0000278057	deg/day
Deimos node rate	0.000000101[illegible]	deg/day
Mars obliquity	0.0006266027	deg

Comparison with ESAPHO/ESADE

To support processing of scientific data from the Soviet "Phobos" mission to Mars in early 1989, Chapront-Touzé[4] developed the ESAPHO semi analytical theory for the motion of Phobos. This theory was later improved[5] and then extended to Deimos (ESADE)[6]. The goal for the internal precision of theory was a few meters over a 20 year period, but for practical matters the form in general release was truncated at the 50 meter level. Because of its semi-analytical nature, the ESAPHO/ESADE theory is not suitable for our needs (i.e., the theory's numerical coefficients need to be regenerated when changes are made in the orbital or dynamic parameters). However, as it provides an alternate representation of the satellite orbits, we tested the extended Sinclair-Morley theory by fitting it to ESAPHO/ESADE over a 100 year interval. We were careful to match the Martian gravity fields and equator orientations as closely as possible in both models (ESAPHO/ESADE employs a ninth order field and accounts for the nutation of the Martian equator). Also we included the secular accelerations as they are inherent in the ESAPHO/ESADE theory. We did, however, suppress the perturbation due to Phobos' figure in ESAPHO[5] because it is not currently included in the extended Sinclair-Morley (the magnitude of this perturbation is quite uncertain but could approach several hundred meters).

Figures 20-25 provide the results of our fit. For Phobos there is agreement in the range of 200 meters. The long period difference in the downtrack is due to the interaction with Deimos which Sinclair-Morley ignores. We attribute the other intermediate period differences to the presence in ESAPHO of additional ignored perturbations (e.g., the higher order Mars gravity field harmonics). For Deimos the differences approach 10 km downtrack and 4 km out of plane. Apparently the amplitude of the long period longitude perturbation differs between the two theories, and significant differences exist in the modelling of the inclination and node perturbations. These three perturbations are primarily due to solar effects. Because the agreement with numerical integration (which has 'exact' solar modelling) is about 500 meters, I suspect that the differences between Sinclair-Morley and ESADE may in fact be due to a problem in ESADE. The latter has not been verified by a long term integration. Moreover, the reference plane in ESAPHO/ESADE is the Mars equator of date rather than the Laplacian plane. Consequently, large long period inclination and node perturbations are present and must be properly taken into account.

Conclusions

In this paper we described an extended Sinclair-Morley analytical theory which will be the model for Martian satellite ephemerides developed at JPL. We outlined the original theory, presented our modifications and additional terms and compared the theory with both numerical integration and the ESAPHO/ESADE theory of Chapront-Touzé. For Phobos it appears that the modelling accuracy approaches 200 meters; the future addition of periodic perturbations due to Deimos and Phobos' figure will improve that accuracy. For Deimos the modelling accuracy is a bit uncertain but is probably at the 1 km level. Any improvement will have to concentrate on a better characterization of the long period solar perturbation as it affects Deimos' mean longitude, inclination, and ascending node. In any event, the current implementation of the theory is more than adequate for the developement of ephemerides which can represent the true satellite orbits with accuracies of only a few tens of km because of observational limitations.

Appendix. Perturbations

Nomenclature

Quantities appearing in the equations which follow, but which have not been defined in the text, are:

J_k	=	the k'th zonal harmonic of the Martian gravity field
η	=	$\sqrt{1-e_0^2}$
l'	=	the mean anomaly of Mars
g'	=	the argument of periapsis of the Martian orbit measured from the intersection of the Martian orbital plane and Martian equator

Secular Perturbations

$$\begin{aligned}
an_0 = \; & n_0 \left\{ \frac{3}{4}\frac{J_2R^2}{p_0^2}\left(1-\frac{3}{2}\sin^2 i\right)\left[2+2\eta-(4+3\eta)\sin^2 I_0+4\sin^4\frac{I_0}{2}\right] \right. \\
& -\frac{15}{8}\frac{J_4R^4}{p_0^4}\left(5-3\eta^2-11\sin^2 I_0\right)\left(\sin^2 i\right)+\frac{3}{16}\frac{J_2^2R^4}{p_0^4}\left(50+20\eta-10\eta^2-165\sin^2 I_0\right) \\
& +\frac{33}{8}\frac{J_3^2R^4}{J_2a_0^4}\left(1-\eta^2\right)\sin^2 I_0+\frac{35}{8}\frac{J_6R^6}{p_0^6}+\frac{189}{4}\frac{J_2^3R^6}{a_0^6}-\frac{315}{8}\frac{J_2J_4R^6}{a_0^6}-\frac{315}{64}\frac{J_8R^8}{p_0^8} \\
& -\frac{1}{4}\left(\frac{n'^2}{n_0^2}\right)\left(1-e'^2\right)^{-3/2}\left(1-\frac{3}{2}\sin^2 I'\right)\left[\left(10-3\eta-3\eta^2\right)\right. \\
& \left.\left.+\frac{3\left(5-20\eta+3\eta^2+6\eta^3\right)}{4\eta}\sin^2 I_0-\frac{3\left(5-3\eta^2\right)}{\eta}\sin^4\frac{I_0}{2}\right]\right\}-\dot{P}\cos I'
\end{aligned} \tag{1}$$

$$
\begin{aligned}
\beta n' &= n_0 \left\{ \frac{3}{2} \frac{J_2 R^2}{p_0^2} \left(1 - \frac{3}{2}\sin^2 i\right) \left[1 - 2\sin^2 I_0 + 2\sin^4 \frac{I_0}{2}\right] \right. \\
&\quad - \frac{15}{16} \frac{J_4 R^4}{p_0^4} \left(7 - 3\eta^2 - 22\sin^2 I - 20\sin^2 i\right) + \frac{3}{16} \frac{J_2^2 R^4}{p_0^4} \left(35 + 12\eta - 5\eta^2 - 116\sin^2 I_0\right) \\
&\quad + \frac{3}{8} \frac{J_3^2 R^4}{J_2 a_0^4} \left(15 - 13\eta^2 - 19\sin^2 I_0\right) + \frac{105}{16} \frac{J_6 R^6}{p_0^6} + \frac{621}{16} \frac{J_2^3 R^6}{a_0^6} - \frac{675}{16} \frac{J_2 J_4 R^6}{a_0^6} - \frac{315}{32} \frac{J_8 R^8}{p_0^8} \\
&\quad \left. + \frac{3}{4} \left(\frac{n'^2}{n_0^2}\right) \left(1 - e'^2\right)^{-3/2} \left(1 - \frac{3}{2}\sin^2 I'\right) \left[\eta - \frac{(5 + 3\eta^2)}{4\eta} \sin^2 I_0 + \frac{(5 - 3\eta^2)}{\eta} \sin^4 \frac{I_0}{2}\right] \right\} \\
&\quad - \dot{P} \cos I'
\end{aligned} \tag{2}
$$

$$
\begin{aligned}
\gamma n' &= n_0 \left\{ -\frac{3}{2} \frac{J_2 R^2}{p_0^2} \left(1 - \frac{3}{2}\sin^2 i\right) \right. \\
&\quad + \frac{15}{32} n_0 \frac{J_4 R^4}{p_0^4} \left(5 - 3\eta^2\right) \left(4 - 7\sin^2 I_0 - 20\sin^2 i\right) \\
&\quad - \frac{3}{16} \frac{J_2^2 R^4}{p_0^4} \left(20 + 12\eta - 2\eta^2 - 18\sin^2 I_0\right) - \frac{3}{8} \frac{J_3^2 R^4}{J_2 a_0^4} \left(21 - 19\eta^2 - 5\sin^2 I_0\right) \\
&\quad - \frac{105}{16} \frac{J_6 R^6}{p_0^6} - \frac{405}{16} \frac{J_2^3 R^6}{a_0^6} + \frac{495}{16} \frac{J_2 J_4 R^6}{a_0^6} + \frac{315}{32} \frac{J_8 R^8}{p_0^8} \\
&\quad \left. - \frac{3}{8} \left(\frac{n'^2}{n_0^2}\right) \left(1 - e'^2\right)^{-3/2} \left(1 - \frac{3}{2}\sin^2 I'\right) \frac{(5 - 3\eta^2)}{\eta} \right\} \cos I_0 - \dot{P} \cos I'
\end{aligned} \tag{3}
$$

Added Perturbations Due to the Martian Gravity Field - J_5

$$\Delta E_2 = +\frac{15}{4} \frac{n_0}{n'} \frac{J_5 R^5}{a_0^5} \frac{(1 + \cos I_0)}{\beta - \gamma} \tan \frac{I_0}{2} \cos \Omega \tag{4}$$

$$\Delta E_3 = -\frac{15}{4} \frac{n_0}{n'} \frac{J_5 R^5}{a_0^5} \frac{(1 + \cos I_0)}{\beta - \gamma} \tan \frac{I_0}{2} \sin \Omega \tag{5}$$

$$\Delta E_4 = \frac{45}{2} \frac{n_0}{n'} \frac{J_5 R^5}{a_0^5} \frac{(1 + \cos I_0)}{\beta - \gamma} e_0 \tan \frac{I_0}{2} \cos (\omega - \Omega) \tag{6}$$

$$\Delta E_5 = +\frac{15}{4} \frac{n_0}{n'} \frac{J_5 R^5}{a_0^5} \frac{\cos I_0}{1 + \cos I_0} \frac{e_0 \cos \omega}{\beta - \gamma} \tag{7}$$

$$\Delta E_6 = -\frac{15}{4} \frac{n_0}{n'} \frac{J_5 R^5}{a_0^5} \frac{\cos I_0}{1 + \cos I_0} \frac{e_0 \sin \omega}{\beta - \gamma} \tag{8}$$

Added Long Period Solar Perturbations

$$
\begin{aligned}
\Delta E_2 &= \frac{3}{8} \frac{n'}{n_0} \left\{ \left[\frac{15 \sin^2 I' \cos^4 \frac{I_0}{2}}{2(1 + 2\beta)} + 3\left(1 - \frac{3}{2}\sin^2 I'\right)\left(1 - \frac{3}{2}\sin^2 I_0\right) \right] e' e_0 \sin (l' + \tilde{\omega}) \right. \\
&\quad \left. + \left[\frac{15 \sin^2 I' \cos^4 \frac{I_0}{2}}{2(1 - 2\beta)} + 3\left(1 - \frac{3}{2}\sin^2 I'\right)\left(1 - \frac{3}{2}\sin^2 I_0\right) \right] e' e_0 \sin (l' - \tilde{\omega}) \right\}
\end{aligned} \tag{9}
$$

$$
\Delta E_3 = -\frac{3}{8} \frac{n'}{n_0} \left\{ \left[\frac{15 \sin^2 I' \cos^4 \frac{I_0}{2}}{2(1 + 2\beta)} - 3\left(1 - \frac{3}{2}\sin^2 I'\right)\left(1 - \frac{3}{2}\sin^2 I_0\right) \right] e' e_0 \cos (l' + \tilde{\omega}) \right.
$$

$$+\left[\frac{15\sin^2 I'\cos^4\frac{I_0}{2}}{2(1-2\beta)}+3\left(1-\frac{3}{2}\sin^2 I'\right)\left(1-\frac{3}{2}\sin^2 I_0\right)\right]e'e_0\cos(l'-\tilde{\omega})\Bigg\} \tag{10}$$

$$\begin{aligned}
\Delta E_5 = \frac{3n'}{8n_0}\Bigg\{&-\frac{159\sin 2I'\cos I}{8(1+\cos I_0)(9-\gamma^2)}e'^3\sin 3l' \\
&+\left[\frac{3\sin^2 I'\cos^2\frac{I_0}{2}}{2(1-2\gamma)}-3\left(1-\frac{3}{2}\sin^2 I'\right)\cos I_0\right]e'\tan\frac{I_0}{2}\sin(l'-\Omega) \\
&+\left[\frac{3\sin^2 I'\cos^2\frac{I_0}{2}}{2(1+2\gamma)}-3\left(1-\frac{3}{2}\sin^2 I'\right)\cos I_0\right]e'\tan\frac{I_0}{2}\sin(l'+\Omega) \\
&+\left[\frac{17(1+\cos I')^2\cos^2\frac{I_0}{2}}{8(2-\gamma)}-\frac{51}{16}\sin^2 I'\cos I_0\right]e'^2\tan\frac{I_0}{2}\sin(4l'+2g'-\Omega) \\
&+\left[\frac{(1-\cos I')^2\cos^2\frac{I_0}{2}}{4(1+2\gamma)}-\frac{3}{4}\sin^2 I'\cos I_0\right]e'\tan\frac{I_0}{2}\sin(l'+2g'+\Omega) \\
&+\left[\frac{7(1-\cos I')^2\cos^2\frac{I_0}{2}}{4(3+2\gamma)}-\frac{7}{4}\sin^2 I'\cos I_0\right]e'\tan\frac{I_0}{2}\sin(3l'+2g'+\Omega)\Bigg\}
\end{aligned} \tag{11}$$

$$\begin{aligned}
\Delta E_6 = \frac{3n'}{8n_0}\Bigg\{&-\frac{53\gamma\sin 2I'\cos I}{8(1+\cos I_0)(9-\gamma^2)}e'^3\cos 3l' \\
&+\left[\frac{3\sin^2 I'\cos^2\frac{I_0}{2}}{2(1-2\gamma)}+3\left(1-\frac{3}{2}\sin^2 I'\right)\cos I_0\right]e'\tan\frac{I_0}{2}\cos(l'-\Omega) \\
&+\left[\frac{3\sin^2 I'\cos^2\frac{I_0}{2}}{2(1+2\gamma)}+3\left(1-\frac{3}{2}\sin^2 I'\right)\cos I_0\right]e'\tan\frac{I_0}{2}\cos(l'+\Omega) \\
&+\left[\frac{17(1+\cos I')^2\cos^2\frac{I_0}{2}}{8(2-\gamma)}-\frac{51}{16}\sin^2 I'\cos I_0\right]e'^2\tan\frac{I_0}{2}\cos(4l'+2g'-\Omega) \\
&+\left[\frac{(1-\cos I')^2\cos^2\frac{I_0}{2}}{4(1+2\gamma)}-\frac{3}{4}\sin^2 I'\cos I_0\right]e'\tan\frac{I_0}{2}\cos(l'+2g'+\Omega) \\
&-\left[\frac{7(1-\cos I')^2\cos^2\frac{I_0}{2}}{4(3+2\gamma)}-\frac{7}{4}\sin^2 I'\cos I_0\right]e'\tan\frac{I_0}{2}\cos(3l'+2g'+\Omega)\Bigg\}
\end{aligned} \tag{12}$$

Added Second Order Perturbation

$$\Delta E_6 = -\frac{9}{16}\frac{n_0}{n'\gamma(1+\cos I_0)}\frac{J_2R^2}{a_0^2}\left[\left(6\frac{J_2R^2}{a_0^2}-25\frac{J_4R^4}{a_0^4}\right)\sin 2i+2\frac{n'^2}{n_0^2}(1-e'^2)^{-3/2}\sin 2I'\right]$$

Acknowledgement

The research described in this paper was performed at the Jet Propulsion Laboratory, California Institute of Technology, under contract with the National Aeronautics and Space Administration.

References

1. Born, G.H, Duxbury, T. C (1975) "The Motions of Phobos and Deimos from Mariner 9 TV Data", *Celest. Mech.* **12**, 77
2. Brouwer, D. (1959) "Solution of the Problem of Artificial Satellite Theory without Drag", *Astron. J.* **64**, 378
3. Brouwer, D., Clemence, G.M. (1961) *Methods of Celestial Mechanics* Academic Press, London
4. Chapront-Touzé, M. (1988) "ESAPHO a semi-analytical theory for the orbital motion of Phobos", *Astron. Astrophys.* **200**, 255
5. Chapront-Touzé, M. (1990a) "Phobos physical libration and complements to the ESAPHO theory for the orbital motion of Phobos", *Astron. Astrophys.* **235**, 447
6. Chapront-Touzé, M. (1990b) "Orbits of the Martian satellites from the ESAPHO and ESADE theories", *Astron. Astrophys* **240**, 159
7. Dobrovolskis, A. R. (1993) "The Laplace Planes of Uranus and Pluto", *Icarus* 105 400
8. Kinoshita, H. (1977) "Third-Order Solution of An Artificial Satellite Theory", Smithsonian Astrophysical Observatory, Special Report 379, Cambridge, MA
9. Kozai, Y. (1959) "The Motion of a Close Earth Satellite", *Astron.* J. **64**, 368
10. Kozai, Y. (1962) "Second-Order Solution of Artificial Satellite Theory without Air Drag", *Astron. J.* **67**, 446
11. Laplace, P.S. (1805) *Méchanique Céleste* v. IV Reprinted in 1966 as *Celestial Mechanics* Chelsea, New York
12. Morley, T.A. (1990) "An improved analytical model for the orbital motion of the Martian Satellites", *Astron. Astrophys.* **228**, 260
13. Sharpless, B.P. (1945) "Secular accelerations in the longitudes of the satellites of Mars", *Astron. J.* **51**, 185
14. Shklovskii, I.S., Sagan, C. (1966) *Intelligent Life in the Universe*, Holden-Day, Inc., San Francisco
15. Sinclair, A.T. (1972) "The Motions of the Satellites of Mars", *Mon. Not. R. Astron. Soc.*, 155, 249
16. Sinclair, A.T. (1989) "The orbits of the satellites of Mars determined from Earth-based and spacecraft observations", *Astron. Astrophys.*, 220, 321

Fig. 2 Phobos Downtrack Differences

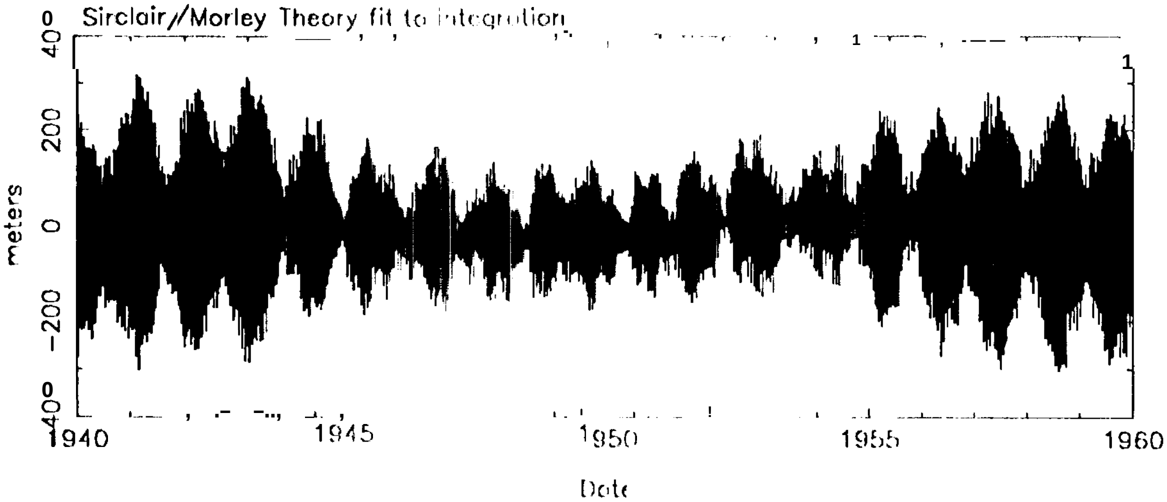

Fig. 3 Phobos Radial Differences

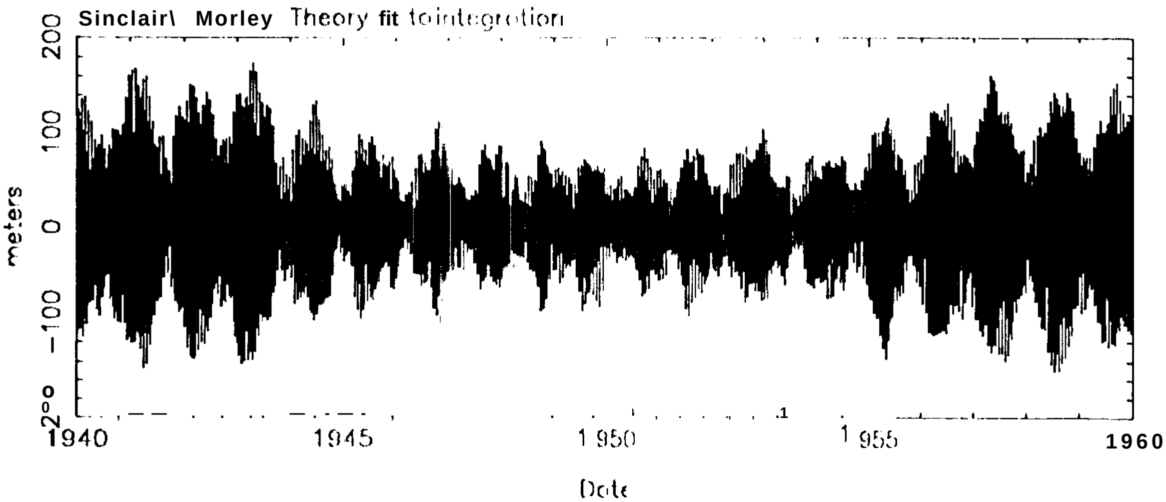

Fig. 4 Phobos Out-of-plane Differences

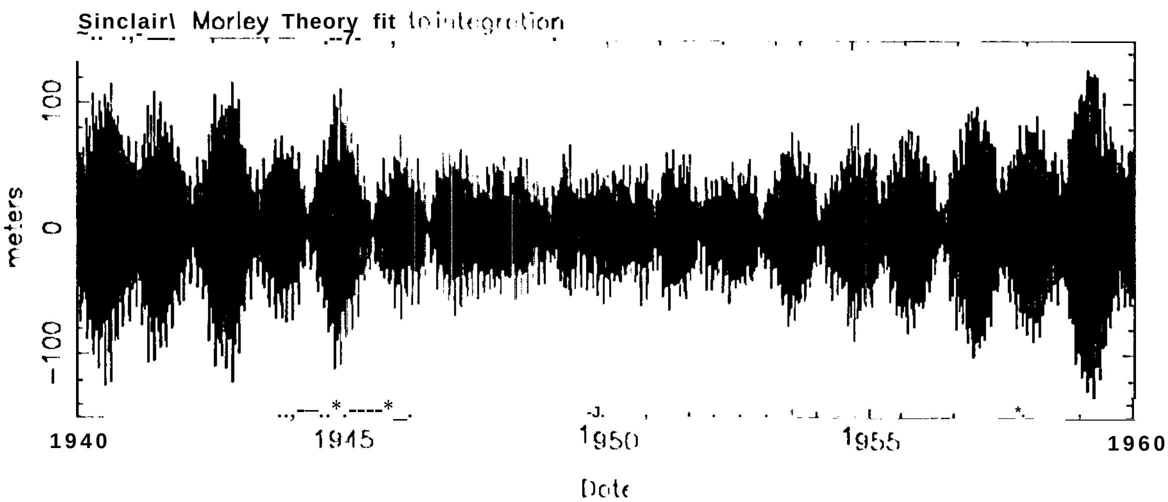

f . 5 Deimos Downtrack Differences

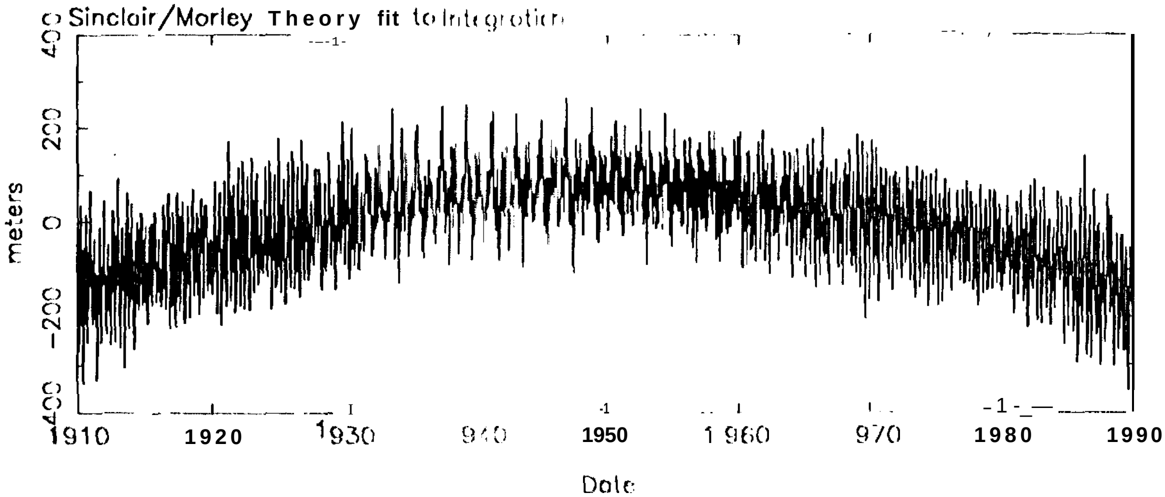

Fig. 6 Deimos Radial Differences

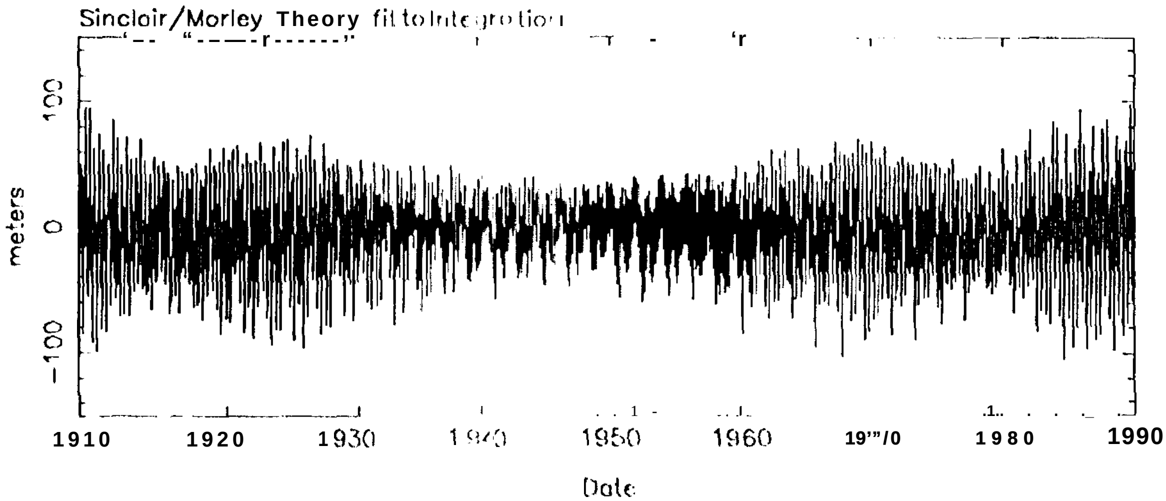

Fig. 7 Deimos out-of-plane Differences

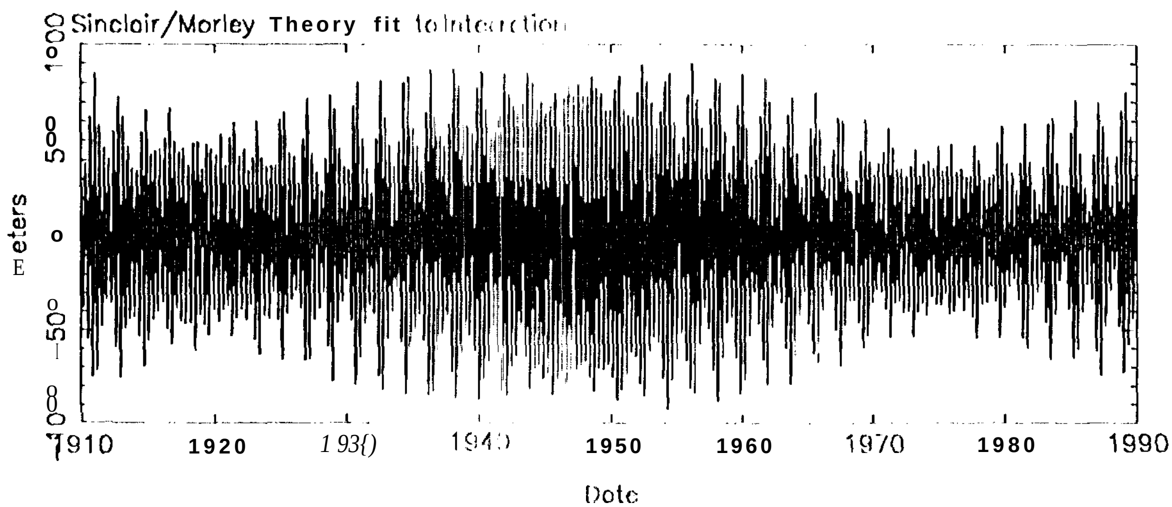

Fig. 8 Phobos Downtrack Differences

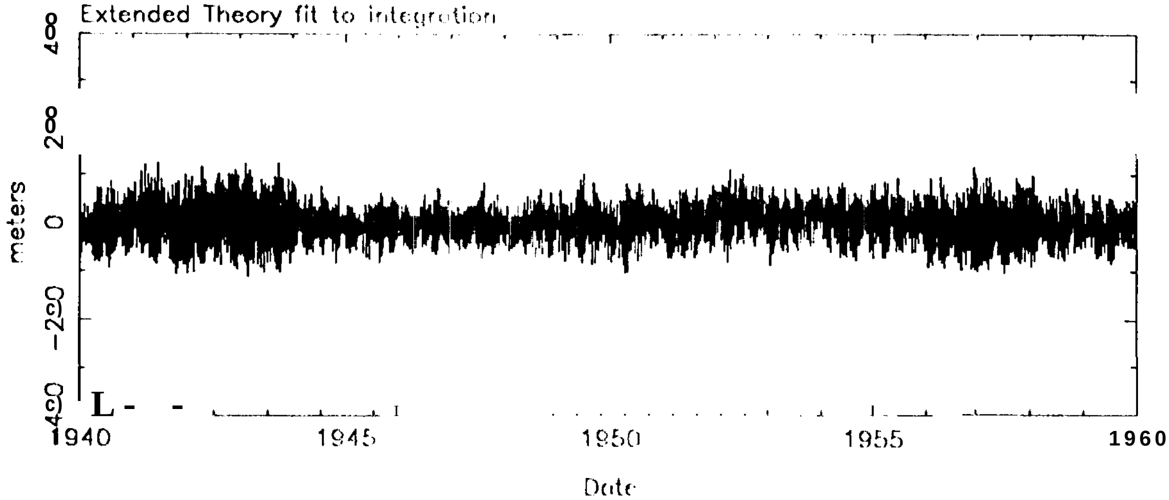

Fig. 9 Phobos Radial Differences

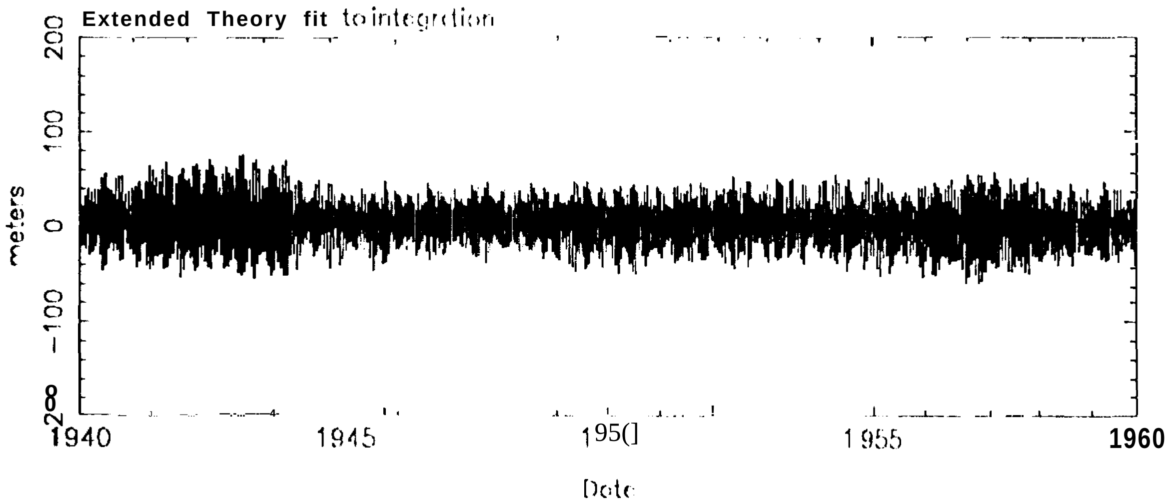

Fig. 10 Phobos Out-of-plane Differences

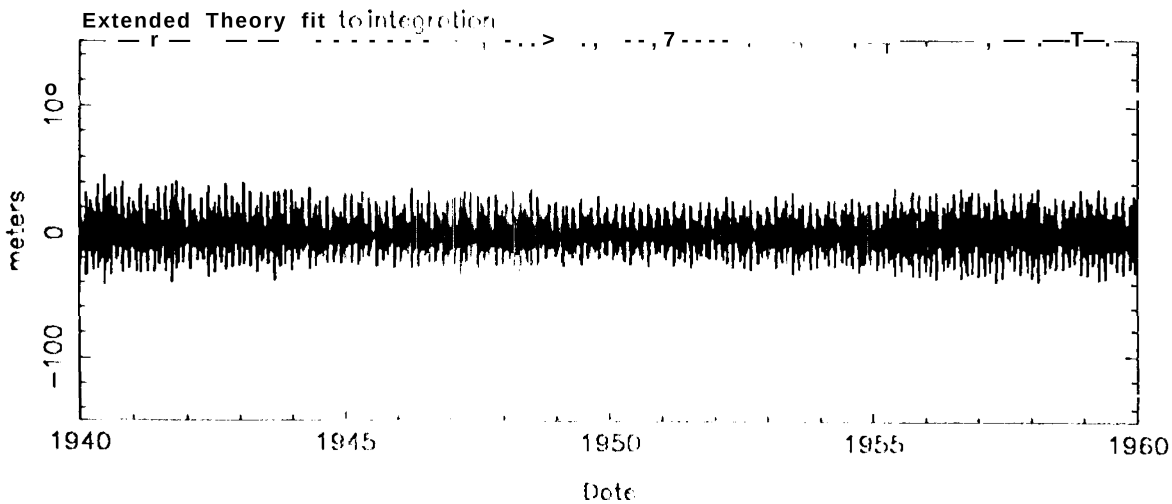

Fig. 11 Deimos Downtrack Differences

Extended Theory fit to Integration

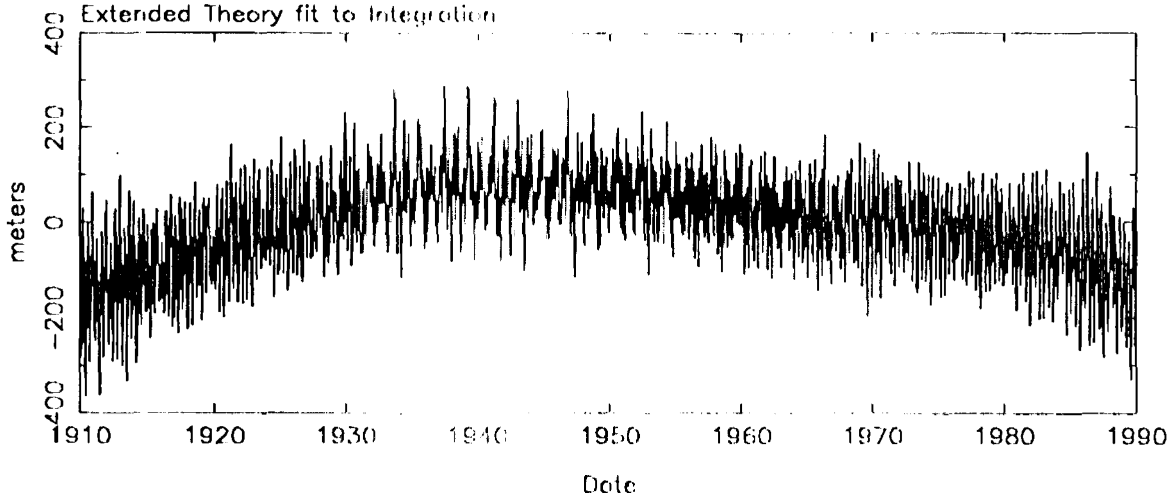

Fig. 12 Deimos Radial Differences

Extended Theory fit to Integration

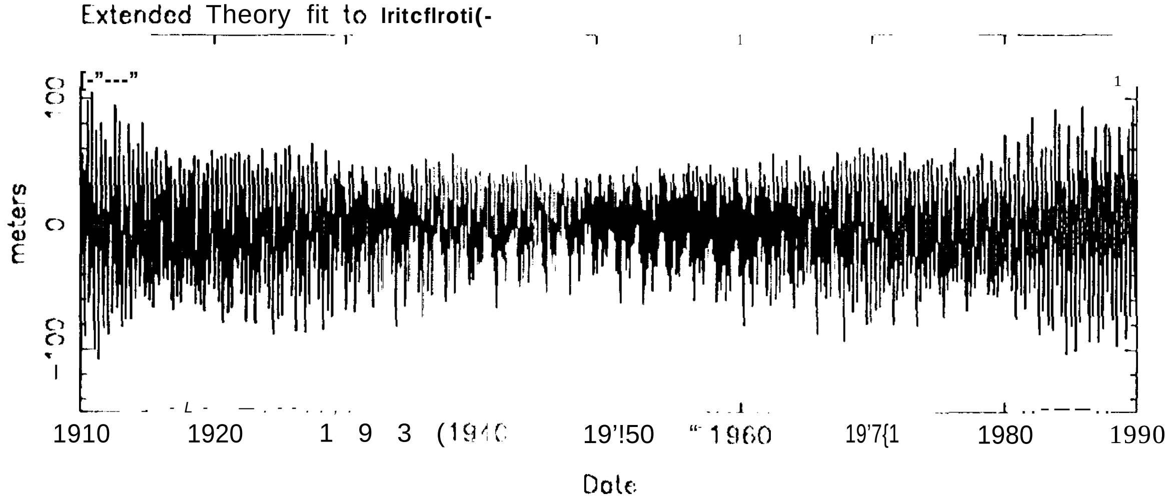

Fig 13 Deimos Out-of-plane Differences

Extended Theory fit to Integration

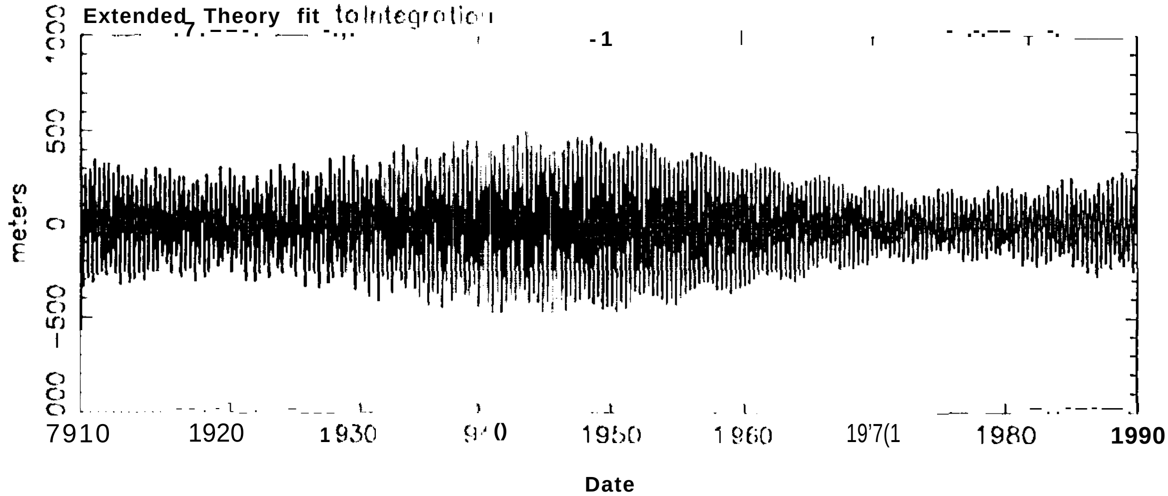

Fig. 14 Phobos Downtrack Differences

Theory fit to Integration with Rate and Equator Corrections

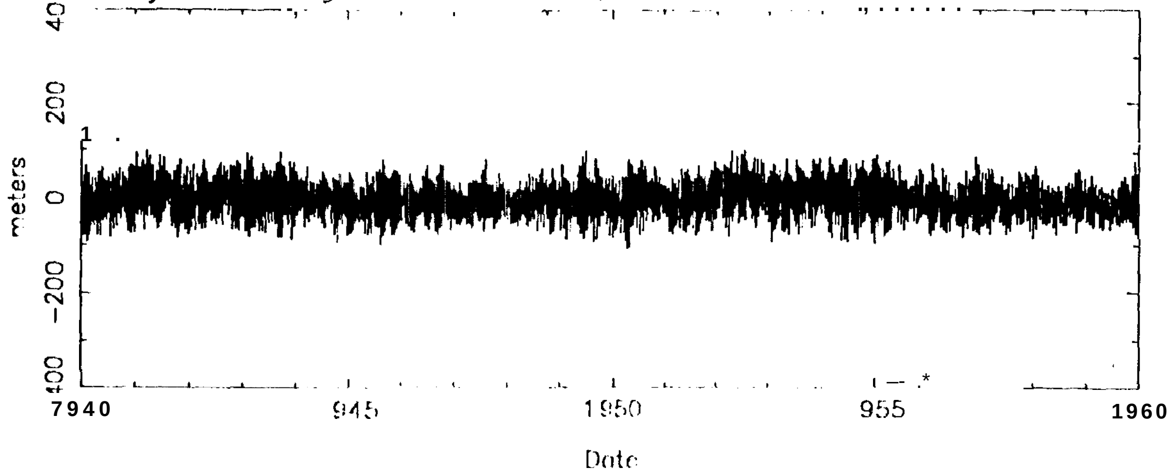

Fig. 15 Phobos Radial Differences

Theory fit to Integration with Rate and Equator Corrections

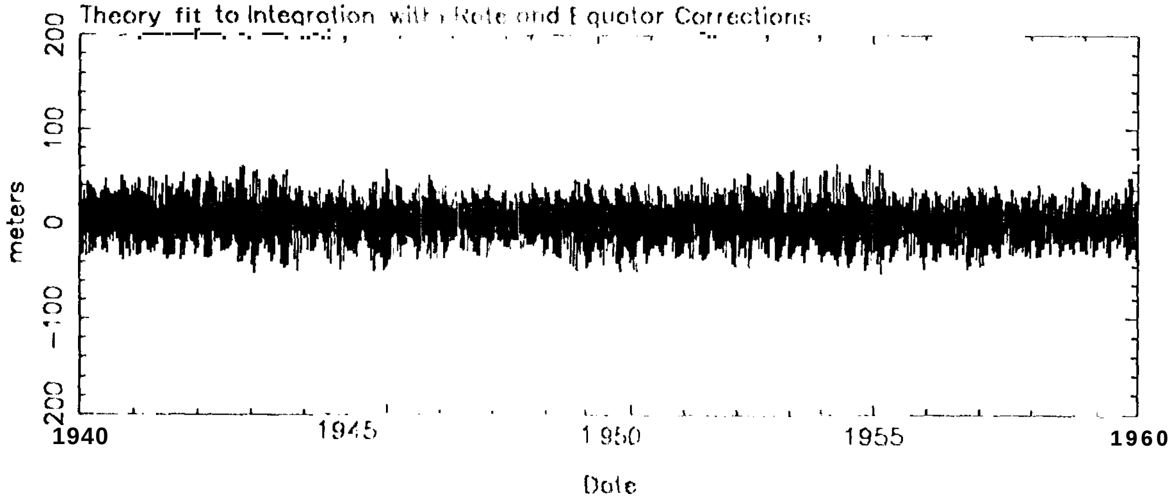

Fig. 16 Phobos Out-of-plane Differences

Theory fit to Integration with Rate and Equator Corrections

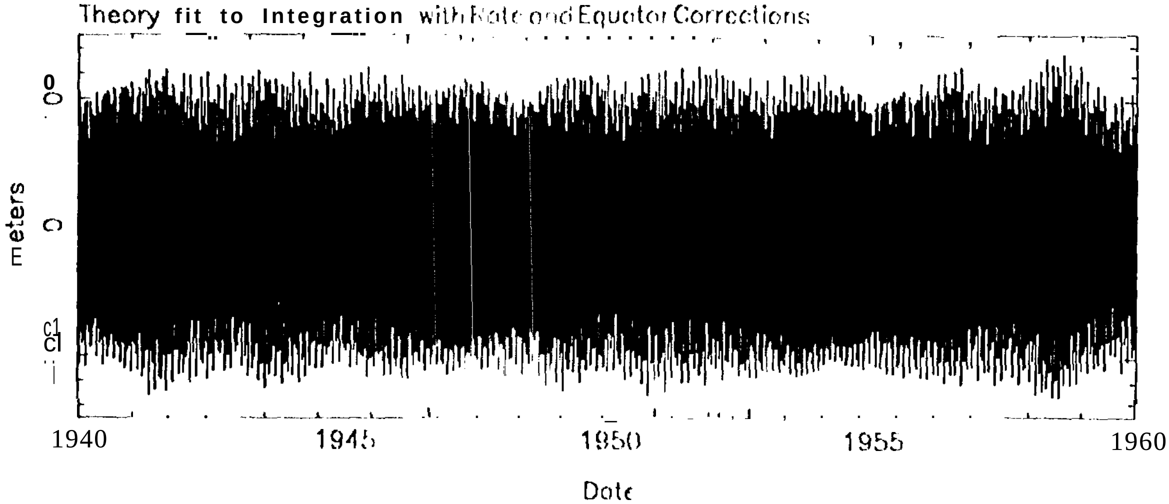

Fig. 17 Deimos Downtrack Differences

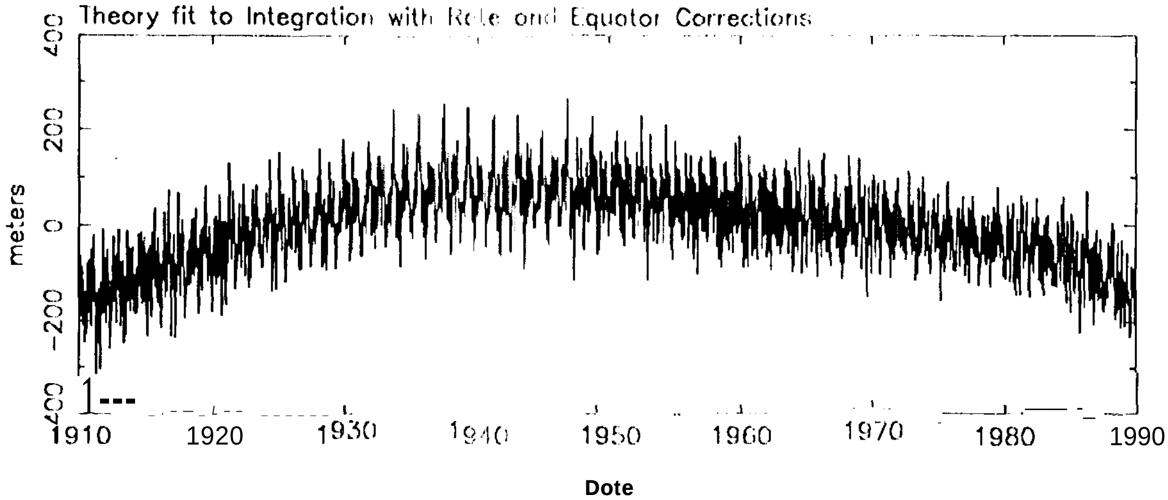

Fig. 18 Deimos Radial Differences

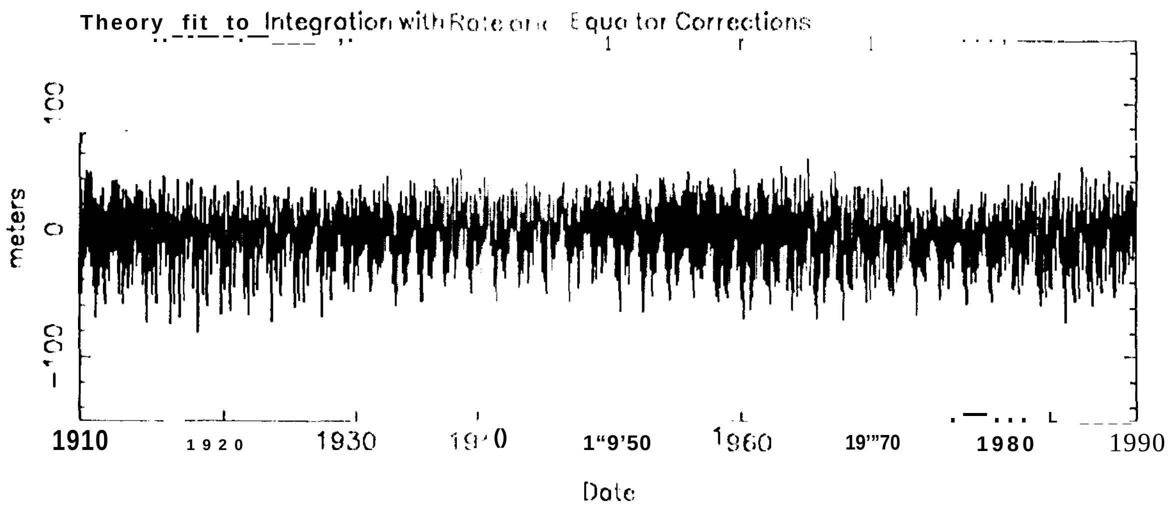

Fig 19 Deimos Out-of-plane Differences

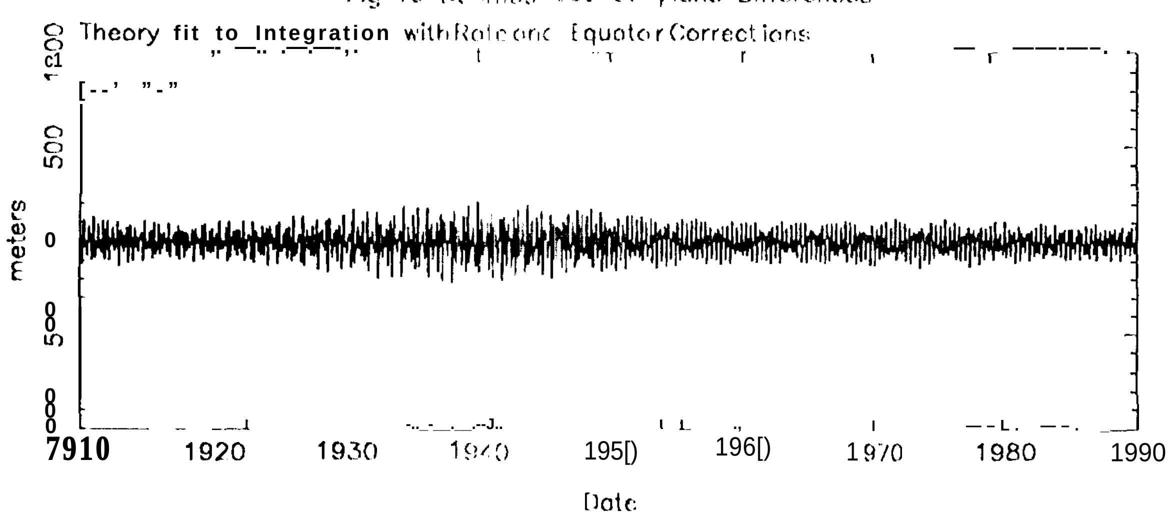

Fig. 20 Phobos Downtrack Differences

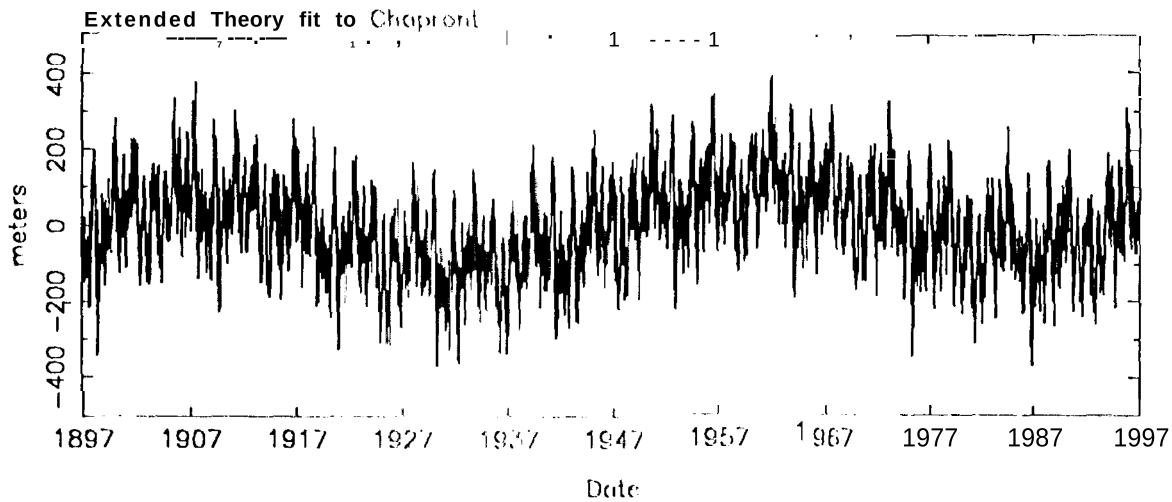

Fig. 21 Phobos Radial Differences

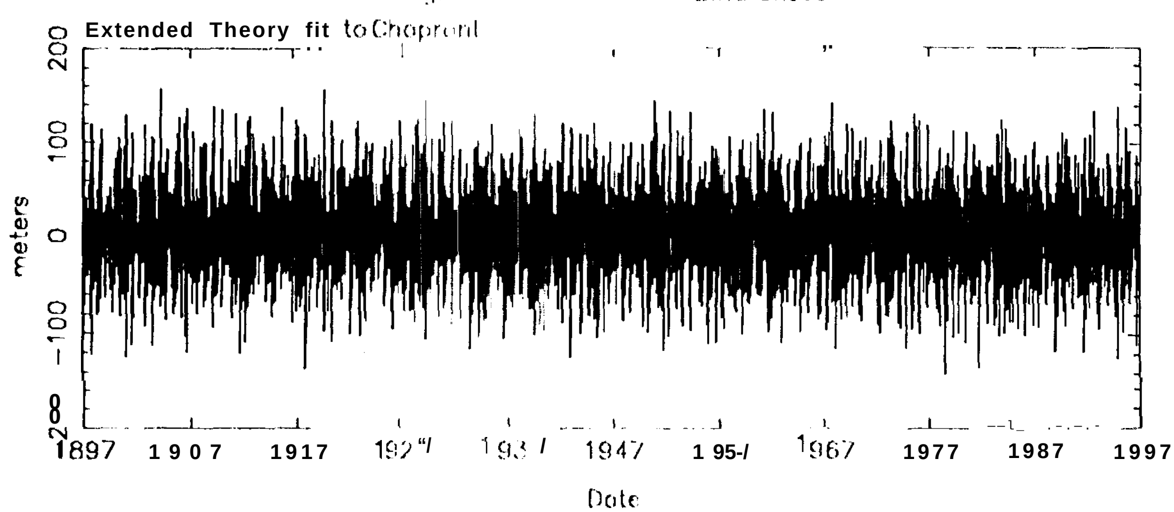

Fig. 22 Phobos Out-of-plane Differences

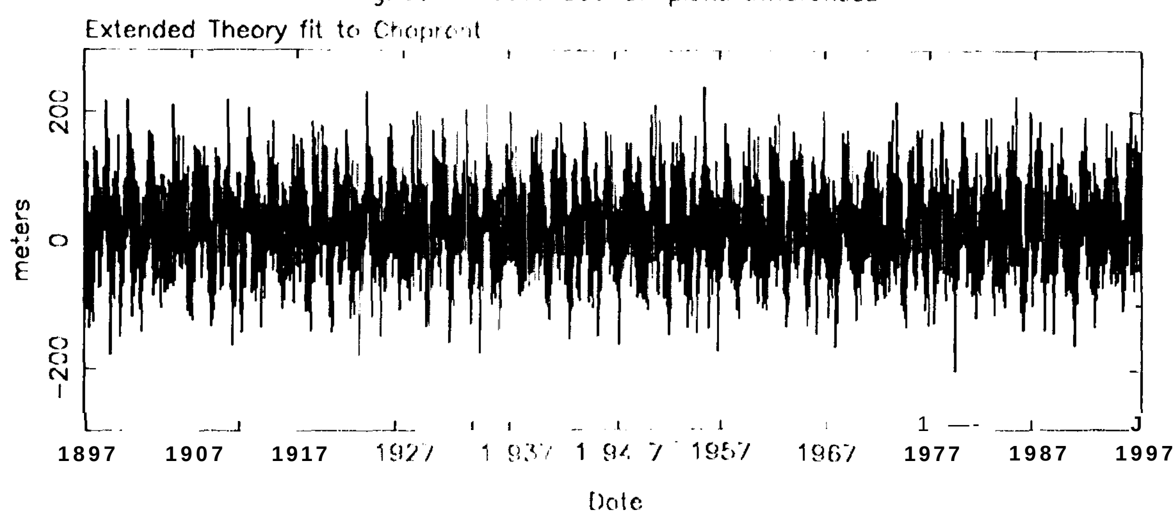

Fig. 23 Deimos Downtrack Differences

Extended Theory fit to Chapront

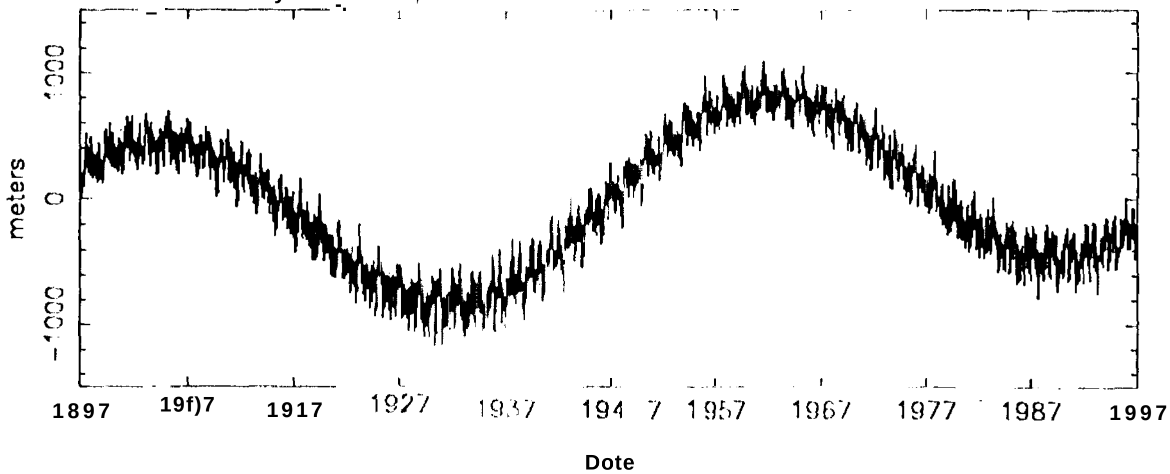

Fig. 24 Deimos Radial Differences

Extended Theory fit to Chapront

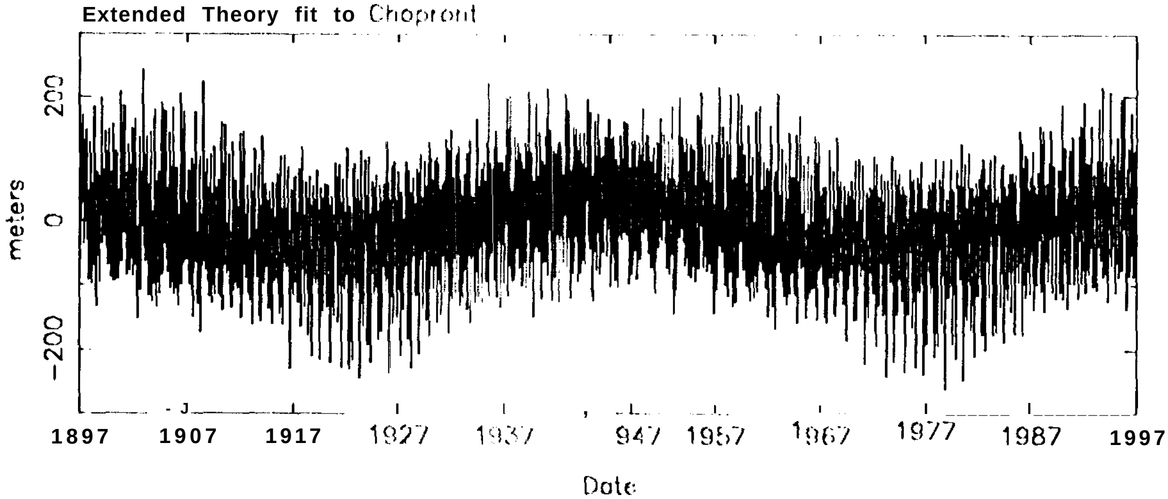

Fig. 25 Deimos Out-of-plane Differences

Extended Theory fit to Chapront